Photophysical and Protonation Time Resolved Studies of Donor-Acceptor Branched Systems With Pyridine Acceptors

Fotis Kournoutas,[1] Kostas Seintis,[1] Nikolaos Karakostas,[2] Jiří Tydlitát,[3] Sylvain Achelle,[4] George Pistolis,[2] Filip Bureš,[3] Mihalis Fakis[1,]*

[1] Department of Physics, University of Patras, Greece, GR-26504, Patras, Greece

[2] NCSR "Demokritos" Institute of Nanosciences and Nanotechnology (INN) 153 10 Athens, Greece

[3] Institute of Organic Chemistry and Technology, Faculty of Chemical Technology, University of Pardubice, Studentská 573, Pardubice, 532 10, Czech Republic

[4] University of Rennes CNRS, ISCR (Institut des Sciences Chimiques de Rennes), UMR 6226, F-35000 Rennes, France

ABSTRACT

A comparative study of the photophysical properties of octupolar pyridyl-terminated triphenylamine molecule, with its quadrupolar and dipolar analogues by means of ambient and low temperature steady state spectroscopy and fs to ns time resolved fluorescence spectroscopy is reported. The push-pull molecules bear triphenylamine electron donating core, pyridine peripheral electron acceptors and acetylenic π-bridge. The samples were studied in solvents of varying polarity and also upon addition of small amounts of acetic acid to induce protonation of the pyridine group. All samples exhibit significant positive fluorescence solvatochromism as well as a relaxation of their excited state to a solvent relaxed Intramolecular Charge Transfer state on the ps timescale. For the octupolar compound, excited state relaxation occurs simultaneously with excitation energy hopping among the branches. The hopping time is solvent polarity controlled since it becomes slower as the polarity increases. The experimental hopping times are compared to those predicted by Förster and Fermi formulations. The samples are capable of emitting broadband light covering almost the whole visible spectrum by careful control of protonation. Energy transfer from the neutral towards the protonated species on the 1 ps timescale is revealed.

INTRODUCTION

Organic molecules with long conjugated backbone and ability for efficient Intramolecular Charge Transfer (ICT) are currently attracting considerable attention as candidates for applications in opto-electronics. Especially, branched molecules show outstanding properties, such as excellent light harvesting and enhanced non-linear optical performance, based on energy localization/delocalization and interbranch interactions.[1-11] Understanding how interbranch interactions, belonging either to the weak or intermediate coupling regime, affect the optical properties, especially within the ultrafast timescale, is of great importance. Depending on the strength of the coupling among branches, coherent and/or incoherent excitation energy transfer (EET) phenomena, taking place on the tens of fs up to the few ps timescale are observed, which are typically followed by ICT and solvent relaxation leading to solvent relaxed CT states.[12-15] It is understood that a plethora of competing dynamic phenomena occur after excitation of the branched compounds with ultrashort laser pulses and their discrimination is not always straightforward.

The photophysics of branched compounds is typically described using the Frenkel exciton model in which the electrostatic interactions among the branches are small compared to the electronic excitation energy.[4,6,16] This model predicts a splitting of the energy levels due to dipole-dipole interactions. In quadrupolar molecules bearing two chromophores attached to a core, the single energy level of the isolated chromophore is split to a set of two one-photon allowed states, lying higher and lower with respect to the energy of the original state. In octupolar ones, where three branches are attached to a core, the model predicts three states. The two lower energy ones are one-photon allowed and have the same energy (degenerate states), while the third one is located at higher energy and has a negligible oscillator strength for one-photon transitions.

The branched molecules either of quadrupolar or octupolar geometry bear an electron donating or accepting core such as triphenylamine (TPA),[4,5,6,16-21] triazine,[5,9,22,23] truxene[24-27] etc. Especially, TPA is the most popular central group in such compounds leading to branched molecules with enhanced electronic coupling and efficient coherent intramolecular EET. On the other hand, various π-deficient heterocyclic electron acceptors such as pyridine,[28,29] pyrazine[30] and pyrimidine[31-33] are incorporated. An interesting way of tuning the photophysics of the molecules bearing the above mentioned π-deficient groups is through protonation, which promotes enhanced ICT as well as red-shifted fluorescence spectra originated by the protonated species.[34-42] EET has been identified as the underlying mechanism in such protonated systems shifting the emission from the blue (emission from the non-protonated species) to the red spectral region (emission from the protonated species).[35,37,38] The above can be also exploited for the generation of white light emitters to be used in White Organic Light Emitting Diodes (WOLEDs) providing an increased interest in these donor-

acceptor molecules with heterocyclic electron acceptors. White light emission can be realized by tuning the protonation so that incomplete EET occurs and both protonated and non-protonated species simultaneously emit. However, the exact dynamics and efficiency of EET especially in solutions has not been studied.

In a recent work of ours, we studied the photophysics of a series of donor-acceptor molecules bearing TPA and -CN moieties as electron donor and acceptor groups, respectively, by means of steady state and time resolved spectroscopy.[43] The goal of the present work is to continue our previous study by investigating a new series of donor-acceptor molecules where the -CN acceptor has been replaced by a pyridine. In addition, the herein studied molecules bear an acetylenic π-bridge. The octupolar compound bearing TPA core and three pyridine groups at the periphery is compared with its quadrupolar and dipolar analogues. Steady state and fs to ns time resolved fluorescence spectroscopy have been used in this study together with low-temperature steady state and anisotropy measurements. Finally, protonation studies have been performed by titration with acetic acid (AcOH). Broad fluorescence spectra covering almost the whole visible spectrum have been observed. The dynamics of the neutral and protonated species have been investigated revealing EET phenomena among the species on the 1 ps timescale.

EXPERIMENTAL

Materials. The chemical structures of the herein studied compounds **1**-**3** are shown in Figure 1. The compounds are of dipolar, quadrupolar and octupolar nature bearing TPA electron donating core and pyridine electron acceptor(s) as well as acetylenic π-bridge. The synthesis and chemical characterization of these compounds has been published in our previous work.[34]

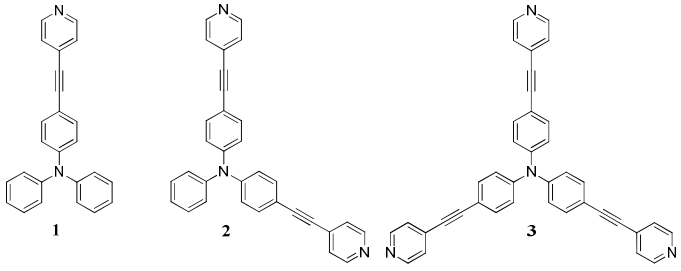

Figure 1. The chemical structures of the herein studied molecules together with their numbering.

Steady State Spectroscopy. The absorption spectra of the samples were measured using a Jasco V-650 UV-Vis spectrophotometer while the fluorescence spectra were detected using a Fluoromax spectrometer (Horiba). For the fluorescence quantum yields (Φ) calculation, 9,10-bis(phenylethynyl)anthracene in cyclohexane was used as standard (Φ= 1.00). For low-temperature measurements, a sealed cryogenic rectangular quartz cuvette was enclosed in a copper block

mounted on the cold finger of a liquid nitrogen cryostat (Oxford Instruments, PE1704). All the low-temperature experiments were performed under a helium atmosphere. Special care was taken to ensure that the glass formed by the frozen solvent was not cracked. To this end, only freshly distilled 2-methyltetrahydrofuran over sodium was used for the preparation of diluted solution of each sample.

Time Resolved Spectroscopy. The fluorescence dynamics were studied on the fs-ps as well as on the ps-ns timescale. For the fs-ps timescale, a femtosecond time resolved upconversion (FU) system has been used using a Ti:Sapphire femtosecond laser (80 fs pulse duration, 80 MHz repetition frequency).[44,45] The second harmonic at 385 nm has been used as the excitation source (less than 1.8 pJ/pulse). The samples were dilute solutions of the chromophores in various solvents placed on 0.8 mm cells with Optical Density of ~ 0.1 at the excitation wavelength. The Instrument's Response Function (IRF) was ~250 fs. The dynamics were detected under magic angle conditions, while anisotropy measurements have also been performed. The fluorescence anisotropy was determined by the equation:

$$r(t)=\frac{I_{par}-I_{per}}{I_{par}+2I_{per}} \quad (1)$$

For detecting I_{par} and I_{per} , a Berek compensator was used to rotate the polarization plane of the fs excitation beam with respect to the polarization plane of the detection, which is prescribed by the optical axis of the upconversion crystal. The parameters of the anisotropy dynamics have been determined by fitting the difference factor $D(t)=I_{par} - I_{per}$ (difference fit) and not the anisotropy itself in order to more accurately determine anisotropy decay times on the 1 ps timescale.[12,46]

For obtaining the ps-ns dynamics, the Time Correlated Single Photon Counting (TCSPC) technique has been used based on a Fluotime 200 spectrometer (Picoquant).[47] The excitation source was a ps diode laser emitting 60 ps pulses at 400 nm. The IRF of the TCSPC spectrometer was ~80 ps. The molecules were investigated in $2.5\text{x}10^{-6}$M solutions in various solvents. The fluorescence dynamics were detected by setting the excitation and detection polarizers to magic angle conditions. The fitting of the decay curves was made by single or bi-exponential functions after careful inspection of the residuals and the χ^2 factor which should be smaller than 1.1. Anisotropy measurements were performed by setting the detection analyzer to horizontal and vertical orientation with respect to the polarization plane of the laser beam. For determining the anisotropy parameters on the ns timescale, the fluorescence intensities polarized parallel and perpendicularly were independently fitted with the anisotropy parameters being used as global parameters for both decays. Before analyzing the curves, the G-factor correction was made.

RESULTS AND DISCUSSION

Steady State Spectroscopy at Ambient and Low Temperature. The steady state absorption and fluorescence spectra of compounds **1**, **2** and **3** have been measured in *n*-hexane (*n*-HEX), toluene (TOL), tetrahydrofuran (THF), chloroform ($CHCl_3$), dichloromethane (DCM), acetone (ACT), dimethylformamide (DMF) and acetonitrile (ACN). The spectra in selected solvents are shown in Figure 2. The photophysical parameters are summarized in Table 1.

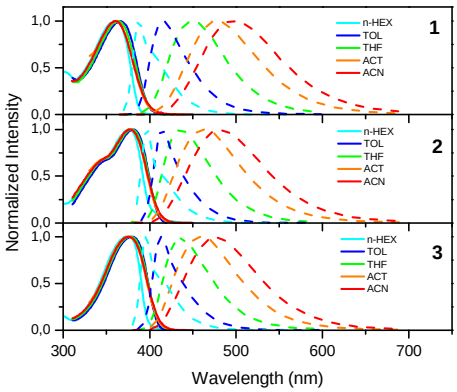

Figure 2. Absorption and fluorescence spectra of **1**, **2** and **3** in selected solvents.

Table 1. Photophysical parameters of **1**, **2** and **3** in various solvents.

Compound	Solvent	λ_{abs} (nm)	λ_{em} (nm)	ϵ ($M^{-1}cm^{-1}$)
1	*n*-HEX	361	388	40300
	TOL	367	415	43700
	$CHCl_3$	371	455	41300
	THF	363	451	32800
	DCM	368	468	42600
	ACT	361	479	38400
	DMF	364	486	42500
	ACN	360	499	41300
2	*n*-HEX	377	397	49300
	TOL	381	414	53000
	$CHCl_3$	386	438	48000
	THF	379	435	44200
	DCM	384	451	51000
	ACT	377	461	44300
	DMF	381	471	52500
	ACN	378	481	46100
3	*n*-HEX	374	396	107900
	TOL	379	413	109500
	$CHCl_3$	384	435	119700
	THF	377	435	98700
	DCM	382	449	126200
	ACT	376	459	96200
	DMF	380	470	130800
	ACN	376	477	110600

Upon increasing the number of branches from **1** to **2**, the absorption spectra exhibit a slight red-shift pointing to a small electrostatic coupling among the two branches in **2**.[48] However, in **3** a small hypsochromic shift, accompanied by a small spectral broadening, are observed in all solvents compared to **2** which may be due to a slight breaking of the degeneracy of the two lower states in the ground state. In all three compounds, the peak as well as the shape of the absorption spectra do not show significant changes when the solvent polarity increases. Figure 3a shows the absorption shift as a function of the solvent function $f(n^2)$ (Table S1 summarizes the solvent properties).

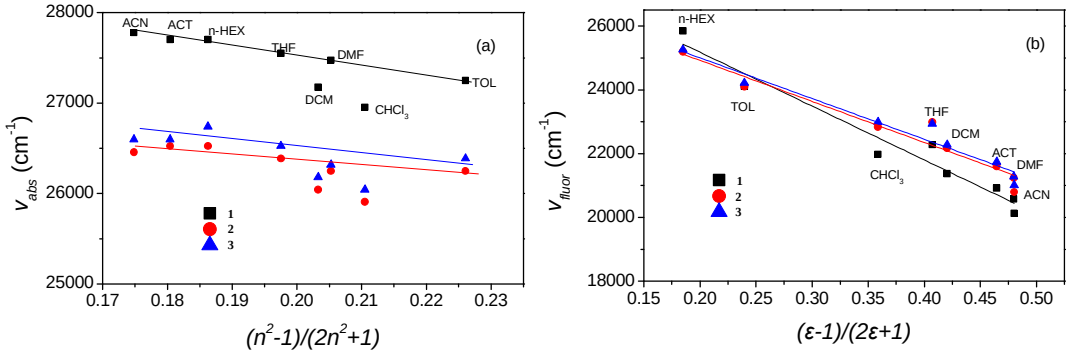

Figure 3. Plot of the solvent shift of absorption (a) and fluorescence (b) peak of the compounds **1**, **2** and **3** as a function of $f(n^2)=(n^2-1)/(2n^2+1)$ and $f(\varepsilon)=(\varepsilon-1)/(2\varepsilon+1)$, respectively.

The dependence of the absorption peak on the $f(n^2)$ points that solvatochromism is mainly governed by dispersion forces.[49,50] However, the results obtained for $CHCl_3$ and DCM do not obey the linear dependence. This can be explained by taking into account that these two solvents have relatively high Kamlet-Taft hydrogen-bond donating ability parameter (α is 0.2 for $CHCl_3$ and 0.13 for DCM)[51] which could lead to H-bonding. Therefore, the bathochromic shift of the absorption peak in these two solvents may be due to special solute-solvent effects. On the other hand, the absorption peaks in ACT and ACN, which also have non-zero α parameter, lay much closer to the regression line. The absorption spectra of **1** and **3** are broad and structureless, while those of **2** exhibit a high energy shoulder which is a manifestation of the splitting of the original excited state due to electronic coupling.[11,42,44,52,53] The coupling energy (V) for **2** was found 1000 cm^{-1} in TOL.[4] This coupling is higher than the one found for similar molecules, but having -CN acceptors instead of pyridine.[43] Table 1 also shows the molar extinction coefficients ϵ of **1**, **2** and **3** in all solvents displaying an increase upon branching. The value of ϵ for **1** is much larger than that of its counterpart molecule having a -CN acceptor[43] which can be ascribed to the enhanced HOMO-LUMO overlap.[34] However, for **2** a 1.5 increase of ϵ vs. **1** was expected while the increase is smaller possibly pointing to structural changes of **2** such as a deviation from the 120^0 angle among the branches. Besides, in **3**, the molar extinction coefficient is almost three times that of **1** indicating

an additive behavior of branches and not a co-operative one where an increase of ϵ of more than three times would be expected.[4,5,11,24]

The transition dipole moment of absorption for **1**, **2** and **3** was determined for TOL, THF and ACN through the equation[54]

$$\mu_{GE}=9.854\times10^{-2}\left[\frac{1}{n}\frac{1}{[f(n)]^2}\int_{S1}\frac{\epsilon(\nu)}{\nu}d\nu\right]^{1/2}$$

where n is the refractive index of the solvent, $f(n)=3n/(2n^2+1)$ and $\epsilon(\nu)$ is the molar extinction coefficient. Integration of the molar extinction coefficient spectrum, for **2**, was made for both the low energy peak and the high energy shoulder. The results of these calculations are shown in Table S2. μ_{GE} increases from 6.72/5.89/6.88D for **1** to 9.76/8.83/9.34 D for **2** and to 11.51/11.04/10.91 D for **3** in TOL/THF/ACN, respectively exhibiting an almost additive behavior of the squared values of the transition moments upon increasing the number of branches.

The fluorescence spectra of all molecules are narrow in the non-polar solvent *n*-HEX, also displaying a low-energy vibronic shoulder. The fact that the fluorescence spectrum is narrower than the absorption one can be primarily ascribed to absorption being due to various rotational conformers (due to the low rotational barrier of the acetylenic linker) and to fluorescence that originates from a geometry relaxed planar state.[55,56] In solvents of increasing polarity, the fluorescence spectra become structureless, broader and bathochromically shifted. This bathochromic shift is significantly more pronounced for **1** displaying the higher polarity of the excited state. The solvatochromic behavior of **3** is interpreted by a lowering of symmetry in the excited state pointing to a localization of energy.[57-59] Figure 3b shows the dependence of the fluorescence peak as a function of $f(\varepsilon)$ (Table S1) which is used instead of the Lippert-Mataga parameter $f(n^2,\varepsilon)$ because dispersion forces are expected to be negligible since significant solvatochromism due to polarity is observed. Here, the peak of the fluorescence spectrum is plotted, instead of the typically used Stokes' shift, because the nature of the ground state (apolar) is different from that of the excited one (polar). In all cases, a linear dependence is observed. The slope is lower for **2** and **3**, compared to **1**, indicating a less polar nature of the branched compounds. This means that excitation is not localized on a single dipolar chromophoric unit, but partially occupies a second branch reducing the dipole moment of the excited state. This conclusion is in agreement with our previous work for compounds with acetylenic linker bearing the -CN acceptors instead of pyridine.[43] However, in other octupolar molecules, where Lippert-Mataga plots[60,61] have been constructed, similar slopes were found for the octupolar and the dipolar molecules meaning that the energy is localized on a single branch prior to emission and the emitting unit is the same in

octupolar and dipolar molecules[4,6,48] while in some cases larger slopes have been observed for the branched compounds.[5,7,15]

The emission transition dipole moment, is calculated by means of the equation[54]

$$\mu_{EG}=1785.7\left[\frac{\Phi}{\tau_F n^3}\frac{1}{[f(n)]^2}\frac{1}{\tilde{\nu}_f^3}\right]^{1/2}$$

where Φ is the fluorescence quantum yield, τ_F the fluorescence lifetime, n the solvent refractive index, $f(n)=3n/(2n^2+1)$ and $\tilde{\nu}_f^3$ is the average cubic fluorescence frequency expressed by:

$$\tilde{\nu}_f^3=\frac{\int I(\nu)\,\mathrm{d}\nu}{\int I(\nu)/\nu^3\mathrm{d}\nu}$$

μ_{EG} can also provide useful information for the nature of the excited state. The calculations have been realized for **1**, **2** and **3** in TOL, THF and ACN and the results are shown in Table S2. μ_{EG} becomes higher upon increasing the branching number from **1** to **2** indicating a delocalized emitting state and an increase in conjugation. On the other hand, μ_{EG} for **3** is smaller than that of **2** but still larger than in **1**. This could possibly indicate that in **3,** a localization of the emitting state on a smaller emitting unit than in **2** occurs. However, the emitting unit in **3** remains larger than in **1** meaning that some of the octupolar symmetry of **3** is retained even in the polar solvent**s**. In general, μ_{EG} for the octupolar molecule is predicted by the Frenkel exciton model to be $(3/2)^{0.5}$ that of the linear one[11] resulting in 7.90/7.63/6.90 D for **3** in TOL/THF/ACN, respectively, which are in reasonable agreement to the experimental ones 7.05/7.09/6.46 D. The differences may be due to the localization of energy to a small emitting unit which is especially mediated by the high polarity solvents. The above relationship between the μ_{EG} values for the linear and octupolar molecules also holds for the lower excitonic state of the quadrupolar one, from where the fluorescence originates. This is also explained by the Frenkel excitonic model for a quadrupolar molecule with θ=120^o between its two branches.[11] Indeed, a comparison of the μ_{EG} values shown above, as predicted by the Frenkel model, with the experimental values found for **2** (Table S2) shows an exceptional agreement.

The steady state absorption and fluorescence spectra at low temperature (95 K) together with steady state excitation and fluorescence anisotropy spectra are shown in Figure 4. In all cases, the absorption spectra are narrower than those measured under ambient conditions due to suppression of a large amount of vibronic modes, while a ~ 20 nm red-shift is also observed (Table S3). This shift can be attributed to the absorption of low energy conformers, which are closer to a more planarized state compared to those at room temperature. In **2**, a clear absorption peak at 350 nm is obvious due to the higher lying state populated due to the splitting of the original state. The

fluorescence spectrum of **1** displays an almost mirror image compared to the absorption in contrast to the behavior observed in the low polarity solvent *n*-HEX where the fluorescence spectrum is narrower than the absorption. This behavior, observed at 95 K, is due to the suppression of planarization in the excited state. In **2** and **3** however, the fluorescence spectra are narrower than the absorption ones meaning that due to their larger molecular size, some of the rotational degrees of freedom leading to planarization are allowed.

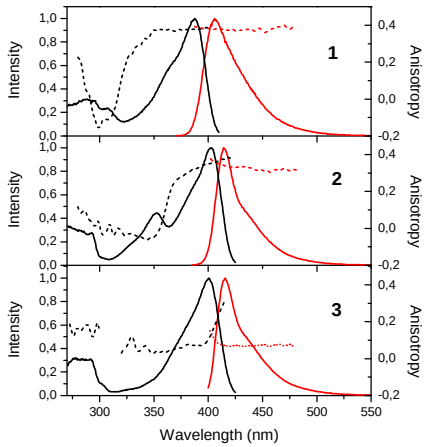

Figure 4. Steady state absorption (solid black lines) and fluorescence spectra (solid red lines) together with steady state excitation (dotted black lines) and fluorescence (dotted red lines) anisotropy spectra of **1**, **2** and **3** at 95 K in 2- methyltetrahydrofuran. The excitation anisotropy spectra were measured by collecting the fluorescence at 415 nm for **1** and at 430 nm for **2** and **3**. The fluorescence anisotropy spectra were detected upon excitation at 375 nm for **1** and at 395 nm for **2** and **3**.

The steady state excitation anisotropy spectra at 95 K are an experimental tool to probe the orientation of transition dipoles of **1**, **2** and **3** avoiding rotational diffusion of chromophores. The anisotropy of **1** is negative for excitation at the $S_2 \leftarrow S_0$ transition (reaching a value of ~ -0.115), while it becomes positive and close to 0.4 when excitation shifts to $S_1 \leftarrow S_0$. The above indicates that the $S_2 \leftarrow S_0$ absorption transition and $S_1 \leftarrow S_0$ emission dipole moments are aligned almost perpendicularly to each other. On the other hand, the $S_1 \leftarrow S_0$ absorption and emission dipoles are parallel to each other as expected for linear chromophores.

The anisotropy spectrum of **2** is clearly different and more interesting. When excitation is made at the high energy state of the split band i.e. at ~ 350 nm, the anisotropy is negative. On the other hand, the anisotropy becomes positive when the excitation is shifted towards the lowest energy state reaching a value of 0.38 at the red side of the spectrum. The negative value of anisotropy at 350 nm is a clear spectroscopic indication of the perpendicular orientation between the transition dipole moments of the two excited states of **2** as predicted by the Frenkel exciton model.[4,5,48,52] When excitation is made at the upper lying state and emission is detected by the lower one, internal

conversion of the energy takes place between the two states before emission. Since rotational diffusion of the molecule is ruled out, the negative anisotropy originates from a substantial rotation of the dipole following this internal conversion between the two states populated after splitting of the original band. For excitation wavelengths longer than 370 nm up to the red edge of the spectrum, the anisotropy increases from 0.2 to 0.38. This is explained by taking into account that as the excitation is shifted to longer wavelengths, the contribution of the higher energy state to the excitation probability becomes smaller. Finally, at the red-edge of the spectrum, excitation is made at the lower energy state, which is also the emitting state, with the absorption and emission transition dipole moments being parallel leading to a high value of anisotropy.[18]

The excitation anisotropy for **3** within the $S_1 \leftarrow S_0$ manifold is constant at 0.05-0.1 over almost the whole spectral range. This is due to energy redistribution among the branches following the excitation of the molecule. In the case of an octupolar molecule with C_3 symmetry, the transition dipole moments of the two lower energy states are perpendicular to each other which, according to the additive law of anisotropy, leads to an anisotropy value of 0.1.[16,62] In our case, the anisotropy value is lower than 0.1 and decreases even more at the short-wavelength edge of the absorption band indicating that the two states are not fully degenerate. This will be further confirmed by the anisotropy value upon red-edge excitation. When the excitation is shifted towards the red-edge of the absorption spectrum, anisotropy increases to a value of 0.3. This would not be observed if emission was due to two degenerate, equally populated states of perpendicular dipoles where a value of 0.1 is expected. Therefore, the two states are not fully degenerate meaning that the molecular symmetry is lowered, while the orthogonality of their dipole moments is retained.[63] Irrespectively of the excitation wavelength, emission always occurs from the lowest energy state. So, in the case of excitation at short wavelengths, energy is transferred between the two non-degenerate states, the emission is depolarized and the anisotropy is lower than 0.1. In the case of excitation at the red-edge, excitation is not expected to experience redistribution pathways i.e. it remains localized at the lower energy state which is also the emitting state and anisotropy is high.

The emission anisotropy spectra of **1**, **2** and **3** are also shown in Figure 4. The anisotropy spectrum of **1** is almost flat and close to 0.4. In **2** and **3**, anisotropy is constant to ~ 0.3 and 0.07 over the whole emission spectrum except from a region at the higher energy part of the spectrum, within the Stokes shift region, where an increase of anisotropy is observed.

Nanosecond Fluorescence Dynamics. The lifetimes of the three chromophores in the ns timescale were determined in order to examine the effect of solvent polarity and branching number. Figure 5

shows the results in *n*-HEX, THF and ACN, while Figure S1 presents the results in TOL, $CHCl_3$, ACT, DCM and DMF. The fitting parameters are summarized in Table S4.

In the non-polar solvent *n*-HEX, the three chromophores show the same lifetime that is close to 1.2 ns. In TOL, **2** and **3** again exhibit almost the same lifetime and almost identical to *n*-HEX, meaning that they experience the same solvent reaction field. On the other hand, **1** exhibits slower dynamics of 1.76 ns. The different decay of **1** indicates that due to its dipolar nature, it experiences a stronger solvent reaction field.

In THF, being a solvent of intermediate polarity, **1** exhibits a bi-exponential decay with two components of 1.13 and 2.84 ns. The first lifetime is almost identical to that found in *n*-HEX and can be ascribed to the Locally Excited (LE) state, while the second one is ascribed to the ICT state populated in THF which is the main emitting state since it has larger amplitude. The behavior of **2** and **3** in THF is markedly different having a fast component of ~ 0.5 ns, with a small amplitude and a longer main one of 1.6-1.7 ns. The main long component is due to an ICT state populated after solvation. The lifetime of the fast component, is much smaller than that of the LE state found in *n*-HEX. Similar bi-exponential dynamics has been found for **1**, **2** and **3** in $CHCl_3$ which is also a solvent of intermediate polarity. The fast component could be primarily ascribed to an LE state which is quenched as the polarity increases leading to a decrease of its lifetime.

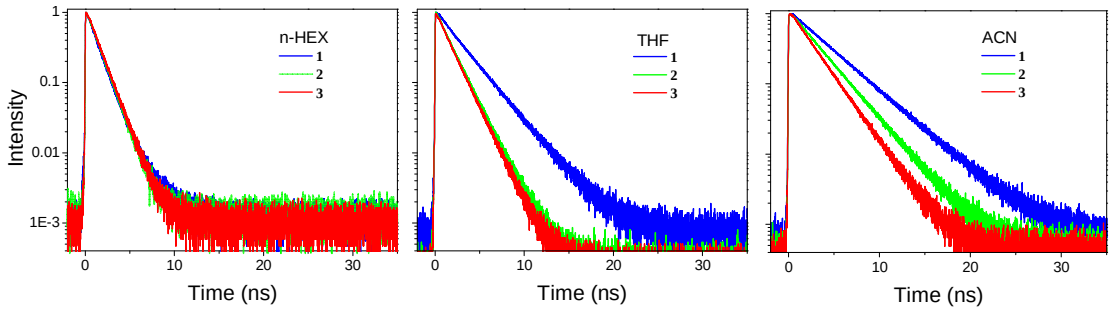

Figure 5. Fluorescence dynamics on the ns timescale for **1**, **2** and **3** in *n*-HEX, THF and ACN ($2.5x10^{-6}$M).

In the most polar solvents DCM, DMF, ACT and ACN all three compounds exhibit single exponential dynamics attributed to the decay of the ICT state being favored in the polar environment. For all compounds, the lifetime of the ICT state in the polar solvents increases with increasing solvent polarity, reaching values of 3.83, 2.83 and 2.32 ns for **1**, **2** and **3**, respectively in ACN, as seen in Figure S2 where the lifetime is plotted as a function of $f(\varepsilon)$. The increase is larger for **1** and smaller for **3** meaning that **1** is more sensitive to the solvent polarity due to its dipolar nature. On the other hand, **2** and especially **3** form a symmetrical non-polar excited state which

gradually turns into an ICT state with increasing solvent polarity. The above results are in qualitative agreement with those found for the compounds having -CN acceptors instead of pyridine.[43] However, smaller lifetimes are found for **1**, **2** and **3** compared to the -CN compounds in polar solvents which agrees to the smaller Stoke's shift, pointing to a less polar excited state for the pyridine compounds.

In previous works on TPA based push-pull molecules, the lifetimes were found to dramatically decrease by more than one order of magnitude after increasing the solvent polarity, while a similar decrease of the fluorescence Q.Y. was also observed leading to a full quenching in polar solvents.[5,16,64] This was ascribed to a change of the nature of the ICT state i.e. to the population of a dark ICT state with a strongly stabilized charge transfer character and an increased non-radiative decay rate mainly due to the energy gap law. Therefore, the existence of various types of ICT states, whose nature was dependent on the solvent polarity, was reported. Those results are in contrast to the results found here. The main difference is that the Q.Y. of molecules **1**, **2** and **3** decrease only by approximately 25% by increasing the solvent polarity from TOL to ACN (ε=2.38 to 36.71) maintaining Q.Y. values of 0.48-0.64 in ACN. This is mainly due to a corresponding decrease of the radiative decay rates which, however, retain in ACN almost 40% of their initial values in TOL (Table S2). On the other hand, the non-radiative decay rate does not significantly change with solvent polarity (Table S2) which clearly implies that the nature of the emitting state remains the same and that the energy gap law does not play a significant role.

Femtosecond Fluorescence Dynamics. To probe the fluorescence dynamics on the fs-ps timescale, the FU technique was used for **1**, **2** and **3** in TOL, THF, ACT and ACN. In TOL, all compounds exhibit a slow rise of fluorescence intensity at all wavelengths except from **1** at the two shortest wavelengths where the intensity is almost constant on the first 20 ps (Figure 6). The above behavior shows that no significant energy redistribution and spectral relaxation takes place. Energy redistribution would be observed in the case where energy is transferred from an LE to an ICT state or in the case where various excited state conformers/rotamers exist. The former is not the case, because of the non-polar nature of TOL where an ICT state is not favored especially in **2** and **3**. On the other hand, the existence of various rotamers in the excited state is ruled out due to a quadratic coupling leading to emitting conformations that are closer to planarity.[56] This is also the reason for the narrow fluorescence spectra in apolar solvents.[43] In THF, wavelength dependent dynamics is observed, where a fast decay at short wavelengths is followed by a slow rise at longer ones (Figure 7). Fitting of the dynamics within the first 20 ps, by a global method, revealed two components, both having positive and negative amplitudes at short and long wavelengths respectively. For **1**, the

time constantswere found 0.60 and 1.8 ps, respectively (Table 2), being slightly slower than the solvation times for THF found by Maroncelli and co-workers for coumarin 153.[65] For **2** and **3**, the lifetimes become slower which is either due to slower solvation owing to their larger molecular size or slower ICT population, because of the lower polarity of their excited state compared to **1**. In ACT and ACN, a similar behavior to THF has been found with lifetimes again attributed to solvation and/or ICT population (Figures S3, S4 and Tables S5, S6).

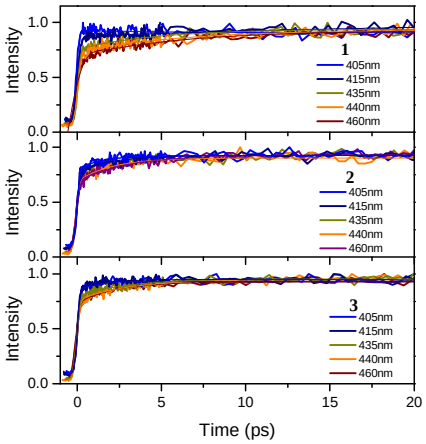

Figure 6. Fluorescence dynamics within the first 20 ps for **1**, **2** and **3** in TOL at various detection wavelengths. exc. 385 nm.

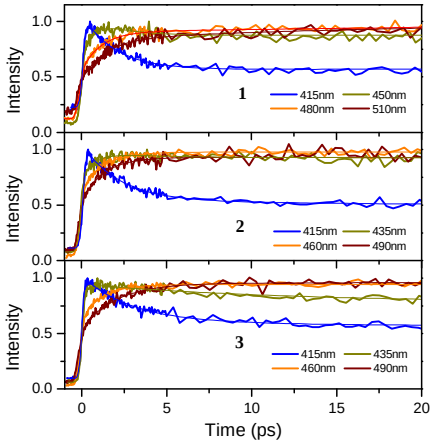

Figure 7. Fluorescence dynamics within the first 20 ps for **1**, **2** and **3** in THF at various detection wavelengths. exc. 385 nm.

Table 2. Fitting parameters of the early dynamics of **1**, **2** and **3** in THF at various detection wavelengths. Excitation was made at 385 nm.

Compound	λ_{det} (nm)	A_1	τ_1 (ps)	A_2	τ_2 (ps)
1	415	0.18	0.60	0.35	1.8
	450	-0.14		0.10	
	480	-0.18		-0.10	
	510	-0.12		-0.25	
2	415	0.13	0.82	0.42	2.9
	435	-0.18		0.07	
	460	-0.22		-0.09	
	490	-0.15		-0.16	
3	415	0.14	1.1	0.32	4.2
	435	-0.18		0.22	
	460	-0.20		-0.05	
	490	-0.16		-0.27	

Femtosecond Anisotropy Dynamics. The fs anisotropy dynamics in *n*-HEX (only for **2** and **3**), TOL, THF, ACT and ACN are shown in Figure 8. An initial anisotropy, r_0, of 0.35-0.38, is observed for **1** in all solvents in agreement with the value found by the low temperature steady state anisotropy measurements for excitation at the $S_1 \leftarrow S_0$ transition. This is close to the maximum value expected for linear molecules in which the absorption and emission transition dipole moments are parallel. The anisotropy of **1** decays on the 100 ps timescale due to rotational diffusion. The correlation times for all molecules were found by means of TCSPC spectroscopy and the results are summarized in Table S7.

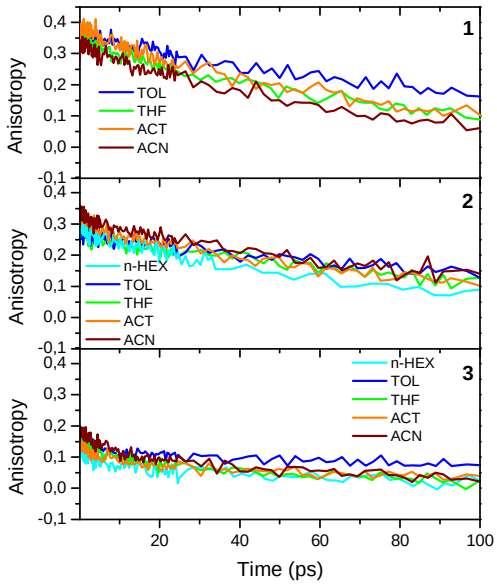

Figure 8. Anisotropy dynamics for **1**, **2** and **3** in *n*-HEX, TOL, THF, ACT and ACN. exc. 385 nm.

Compound **2** has a reduced r_0 of 0.25-0.30. As discussed before, band splitting occurs in the case of quadrupolar systems due to a strong coupling between the linear branches. Upon exciting at 385 nm (which is the excitation wavelength for our FU measurements), mainly the lower energy state of the coupled system is populated. However, if that was the case, then we would expect an r_0 value close to 0.4. Therefore, it is concluded that the decrease of the r_0 in **2** compared to **1** is an indication that the higher energy state of the split band is also populated to some extent. The anisotropy dynamics of **2** reveal a main long component due to rotation (Table S7), but also a secondary component with a few ps time constant is observed. This component, which has a ~ 10 % contribution to the anisotropy decay, is ascribed to energy hopping among the branches. A detailed investigation of the energy hopping will be made for the octupolar molecule **3** (vide infra).

On the other hand, **3** exhibits a significantly reduced r_0 of 0.1-0.17 in the five solvents. The anisotropy starts decreasing on the 1-10 ps timescale. The absence of a depolarization component on the 10 fs timescale points that a coherent energy delocalization mechanism is not observed. Instead, the observation of an initial anisotropy close to 0.1 indicates that the coherent mechanisms take place faster than our IRF. The anisotropy decay on the ps regime shows the depolarization after the coherent mechanism takes place. Depolarization due to coherent mechanism was observed for other TPA based octupolar systems on the 10 fs timescale[66-68] while in the case of molecules with truxene and benzene core, a slower coherent anisotropy decay was reported.[5,12,54] In our systems, we attribute the depolarization on the 1-10 ps timescale to incoherent hopping among the branches which changes the orientation of the emission dipole. The fitting results of the anisotropy in the ps timescale are summarized in Table 3. Specifically, the depolarization times have been found 2.5±0.5, 3.2±0.4, 4.1±0.7, 5.0±0.7 and 7.0±0.9 ps for *n*-HEX, TOL, THF, ACT and ACN, respectively. It is obvious that the anisotropy decay time increases as the solvent polarity increases. This can be explained by taking into account that the solvation process occurs faster or simultaneously with the hopping mechanism.[13] In *n*-HEX and TOL, solvation is not operative and the fluorescence spectrum is narrow and located at short wavelengths, thus increasing the spectral overlap with the absorption spectrum. This leads to an increased hopping rate i.e. short hopping time. On the other hand, in polar solvents such as THF, ACT and ACN, the solvated state exhibits a red-shifted spectrum decreasing the spectral overlap. Thus longer hopping times are expected in polar solvents if the solvated state participates in the hopping process. This is experimentally found here where the hopping time increases twice in ACT and almost three times in ACN compared to *n*-HEX. The solvation times for THF, ACT and ACN have time constants of 1.09, 1.52 and 0.63 ps, with almost 50 % pre-exponential factors.[65] This means that solvation in these solvents is 3-5 times faster than hopping. If solvation takes place much faster than hopping, then only the solvated state

participate in EET among branches. In our case, we believe that solvation and hopping are kinetically competing mechanisms so that hopping takes place during solvation from both the unsolvated and the solvated states.

Table 3. Experimental anisotropy decay times for **3** in *n*-HEX, TOL, THF, ACT and ACN as well as the theoretically predicted decay times via the Förster and Fermi formulation for TOL, THF and ACN.

Compound	Solvent	τ_{dep}^{exp}(ps)	$\tau_{dep}^{Förster}$(ps)	τ_{dep}^{Fermi}(ps)
3	*n*-HEX	2.5±0.5		
	TOL	3.2±0.4	0.23	0.19
	THF	4.1±0.7	0.83	0.82
	ACT	5.0±0.7		
	ACN	7.0±0.9	1.06	1.32

The anisotropy decay time τ_{dep} is related to the EET time by the equation $\tau_{dep}=\tau_{EET}/4(1\text{-}cos^2\theta)$ which in the case of octupolar compounds with θ=120° among the branches, becomes $\tau_{dep}=\tau_{EET}/3$.[68,69] By employing the Förster point-dipole approximation,[70] τ_{dep} is found 0.23, 0.83 and 1.06 ps for TOL, THF and ACN with κ=1.75 i.e if the chromophores are considered to have a constant angle θ =120° among them and 1.04, 3.83 and 4.86 ps for TOL, THF and ACN with κ^2=2/3 i.e if all possible orientations of the chromophores are taken into account (see the SI for details on the formulation used and calculations). Although the τ_{dep} values calculated by averaging over all orientations are in good agreement with the experimental results, the Förster model is not accurately employed here, because of the small distance between energy donor and acceptor, which may also experience through bond interactions via the common central core.

Besides, the τ_{EET} used to calculate the τ_{dep} can also be found via the Fermi's golden rule (see SI for details).[71,72] The electronic coupling, *V*, needed for the determination of τ_{EET} has been calculated using the dipole moments of **1** presented in Table S2 and found 256, 236 and 260 cm^{-1} for **3** in TOL, THF and ACN, laying in the very weak coupling regime. Finally, the values of τ_{dep} predicted via the Fermi's golden rule for **3** in TOL, THF and ACN are 0.19 and 0.82 and 1.32 ps, respectively (Table 3).

Protonation Studies. The effect of protonation on the optical properties of compounds **1** and **3** was studied by titration with AcOH. The protonation site in **1** and **3** is the pyridine nitrogen, making the protonated pyridine a stronger electron withdrawing group than the neutral one.[73] Figures 9a and c show the absorption spectra of **1** and **3,** respectively, in $CHCl_3$ solutions ($2.5x10^{-6}$M) by adding various amounts of AcOH. The absorption spectra show a progressive bathochromic shift as well as

the appearance of a shoulder at ~ 450 nm which is attributed to the protonated species.[34] It is noted that in a previous work, the protonation of **3** has been studied using TFA acid instead of AcOH and a more intense absorption band at 450 nm was observed due to the stronger nature of the acid used.[34] The fluorescence spectra of **1** and **3** upon addition of acid are shown in Figures 9b and 9d. The main fluorescence band at 435/445 nm for **3**/**1** decreases and a new, broad fluorescence band with a peak at 580/600 nm for **3**/**1** emerges, as the amount of acid increases. Since the protonation site is the nitrogen at the pyridine segment, the intensity of the acid generated fluorescence band is more intense for **3** than for **1,** which is due to the three pyridine groups in the former. However, it is also observed that for **3** the fluorescence intensity at 580 nm is saturated when the amount of AcOH exceeds 20 μL. The excitation spectra of **1** and **3** upon detection of the fluorescence at the low-energy band of the protonated species are shown in Figure S5. They are similar to the absorption ones and provide a first evidence that emission of the protonated species is due not only to their direct excitation at 450 nm, but also due to EET transfer from the neutral molecules which are excited at 380 nm. A more thorough investigation of the EET between neutral and protonated species is realized by means of fs spectroscopy.

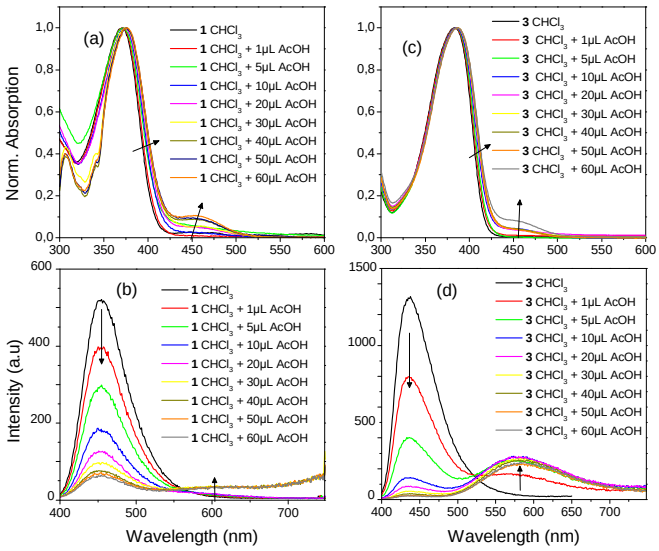

Figure 9. Steady state absorption (a) and (c) and fluorescence (b) and (d) spectra of **1** and **3** upon addition of various amounts of AcOH in **3** ml $CHCl_3$ solutions ($2.5x10^{-6}$M). The excitation wavelength for the fluorescence spectra was 380 nm. The arrows show the change of the spectra by increasing the amount of AcOH.

The fluorescence dynamics within the first 20 ps for **1** and **3** detected at both the short and long wavelength peaks, upon adding AcOH, are shown in Figure 10. The fluorescence of the neutral species of **3** at 435 nm decays faster upon protonation compared to the decay in $CHCl_3$ solutions without AcOH, in agreement with the quenching observed in the steady state spectra. In addition, the dynamics of **3** at 580 nm, where the protonated species emit, exhibits a slow rise. By globally

fitting the dynamics at 435 and 580 nm, a common lifetime of 1.9 ps is found pointing to an EET process from the higher energy neutral to the lower energy protonated species. The same behavior is also observed for **1** where the fitting procedure gave an EET lifetime of 0.7 ps.

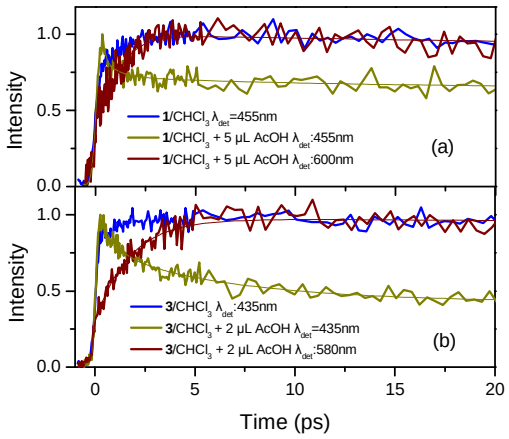

Figure 10. Fluorescence dynamics for (a) **1** and (b) **3** in $CHCl_3$ within the first 20 ps, with and without AcOH, at emission wavelengths corresponding to the fluorescence bands of the neutral and protonated species. exc. 385 nm.

The observation of an EET process between the neutral and acid generated protonated species based on the fs dynamics is in agreement with previous reports[35,37,38] and unambiguously points that the two species are found close to each other facilitating EET. If the neutral and protonated species are isolated and free to diffuse inside the solutions, then EET would not be possible due to the large average distance among them. Therefore, it is understood that complex molecules comprising both species exist in the solutions, in which the donor-acceptor distance is small and EET is operative. To investigate more thoroughly the above assumption, we performed ns anisotropy measurements in $CHCl_3$ solutions of **1** and **3** upon addition of AcOH (Figure S6). When the detection wavelength of the fluorescence anisotropy is at the low-energy peak, i.e. at the emission band of the protonated species, a significant increase of the correlation time is found. More specifically, the correlation time for **3** at 580 nm increases upon adding AcOH from 0.21 ns in pure $CHCl_3$ solutions to 0.42, 0.45 and 0.50 ns for 1, 5 and 20 μL of AcOH, while it remains constant upon further increasing the quantity of acid. This means that emission at the low-energy spectral region originates from large complex molecules in which EET is operative verifying our initial assumption. Apart from the increase of the rotational time, an increase of the initial anisotropy of **3** is also observed at the low-energy band (r_0=0.15 at 580 nm for the solutions with AcOH) compared to that found at the high energy one (r_0=0.11 at 435 nm for the solutions with and without AcOH) which is due to the neutral species (Figure S6b). This points to a smaller depolarization of the emitted light and to a less efficient redistribution of energy. This is plausible taking into account that energy is absorbed by the neutral molecules (excitation at 400 nm), but before it is delocalized among the branches

leading to depolarization and decrease of initial anisotropy, it is transferred and becomes localized on the energy-acceptor protonated species which are also the emitting species. Identical behavior is observed for **1**, where the rotational time increases from 0.16 ns in $CHCl_3$ solutions to 0.26 ns when AcOH is added (Figure S6a).

To determine the lifetime of the protonated species, magic angle ns fluorescence dynamics were investigated at the low energy fluorescence band upon addition of AcOH. Figure S7a shows the results for **3** at 580 nm. The lifetime of the protonated species in $CHCl_3$ with 1 μL AcOH was found 2.3 ns i.e. longer than that of the neutral species in pure $CHCl_3$ solutions which exhibit an average lifetime of 1.5 ns (Figure S7a inset shows a comparison of the dynamics without and with 1 μL of AcOH). However, upon increasing the amount of acid, the lifetime decreases reaching a value of 1.45 ns for 60 μL AcOH. This decrease of the protonated species lifetime is in agreement with the saturation of the fluorescence intensity upon adding AcOH, as found by steady state spectroscopy, and may be ascribed to the stronger ICT since the electron accepting ability of the protonated pyridine increases. The dynamics of the neutral species after addition of AcOH is shown in Figure S7b. It is obvious that the dynamics is dramatically accelerated and the average lifetime is reduced from 1.44 ns without AcOH to 0.36 ns for 30 μL of AcOH. This decrease of the lifetime is in agreement to the results made by the FU method and again indicate the quenching of the neutral species as the amount of AcOH increases.

To conclude with the protonation studies of compounds **1** and **3**, an investigation of the steady state, fs and ns time resolved data of the protonated solutions of **1** and **3**, illustrates that: i) large complex molecules are formed incorporating neutral and protonated species upon addition of acid, ii) EET is operative from the neutral to the protonated species within these complex molecules leading to red-shifted emission, iii) the lifetime of the large molecular species emitting at the red-shifted band decreases with the amount of AcOH leading to a saturation of their fluorescence intensity. The above are important findings towards understanding the origin of the fluorescence in protonated species which lead either to red-shifted or even to white-light emission.

CONCLUSIONS

The photophysical properties of an octupolar molecule (**3**) bearing TPA as central core and pyridine substituents have been studied and compared to those of its quadrupolar (**2**) and dipolar (**1**) analogue. A typical solvatochromic shift of the fluorescence spectra was observed for all molecules, while the largest Stoke's shift was found for the dipolar D-π-A molecule indicating the strongest dipolar excited state. This molecule also exhibits the longest ICT state lifetime. Steady state spectra at 95 K clearly revealed a split band for **2** due to electrostatic coupling between the two branches.

The two excited states populated in **2** exhibit almost perpendicular dipoles as found by steady state anisotropy spectra. For **3**, the steady state anisotropy spectra showed that the lowest energy states are not fully degenerate. Anisotropy dynamics on the fs-ps timescale for **3** showed that incoherent EET among branches is operative on the 2.5 -7.0 ps timescale depending on solvent. The hopping mechanism becomes slower as the solvent polarity increases due to the much reduced spectral overlap of the absorption and the fluorescence spectrum of the ICT state. The experimental EET lifetimes are in reasonable agreement with those theoretically predicted by means of Förster and Fermi formulations. Finally, the effect of protonation upon adding AcOH in $CHCl_3$ solutions on the photophysical properties was studied in order to investigate possible EET phenomena among the neutral and protonated species. It was found that EET is operative with less than 2 ps lifetime within large molecules which are formed after interaction of the electron richer (nonprotonated) and electron poorer (protonated) molecules.

ASSOCIATED CONTENT

Supporting Information

The Supporting Information is available free of charge on the ACS Publications website at
Details on the calculations, tables with photophysical data, stationary spectra and additional time-resolved dynamics

AUTHOR INFORMATION

Corresponding Author

* Mihalis Fakis. Tel: +30 2610 996794. E-mail: fakis@upatras.gr

ORCID

Mihalis Fakis: 0000-0003-0801-7029
Filip Bureš: 0000-0002-2832-6673
Sylvain Achelle: 000-0002-9226-7735

REFERENCES

1 Hrobárik, P.; Hrobáriková, V.; Sigmudová, I.; Zahradnik, P.; Fakis, M.; Polyzos, I.; Persephonis, P. Benzothiazoles with Tunable Electron-Withdrawing Strength and Reverse Polarity: A Route to Triphenylamine-Based Chromophores with Enhanced Two-Photon absorption. *J. Org. Chem.*, **2011**, *76*, 8726-8736.

2 Cvejn, D.; Michail, E.; Polyzos, I.; Almonasy, N.; Pytela, O.; Klikar, M.; Mikysek, T.; Giannetas, V.; Fakis, M.; Bureš, F. Modulation of (Non)linear Optical Properties in Tripodal Molecules by Variation of the Peripheral Cyano Acceptor Moieties and the π-Spacer. *J. Mater. Chem. C*, **2015**, *3*, 7345-7355.

3 Jia, M.; Ma, X.; Yan, L.; Wang, H.; Guo, Q.; Wang, X.; Wang, Y.; Zhan, X.; Xia, A. Photophysical Properties of Intramolecular Charge Transfer in Two Newly Synthesized Tribranched Donor-π-Acceptor Chromophores. *J. Phys. Chem. A*, **2010**, *114*, 7345-7352.

4 Katan, C.; Terenziani, F.; Morgin, O.; Werts, M.H.V.; Porrès, L.; Pons, T.; Mertz, J.; Tretiak, S.; Blanchard-Desce, M. Effects of (Multi)branching of Dipolar Chromophores on Photophysical Properties and Two-Photon Absorption. *J. Phys. Chem. A*, **2005**, *109*, 3024-3037.

5 Liu, C.; Tang, K.C.; Zhang, H.; Pan, H.A.; Hua, J.; Li, B.; Chou, P.T. Studies of Excited-State Properties of Multibranched Triarylamine End-Capped Triazines. *J. Phys. Chem. A*, **2012**, *116*, 12339-12348.

6 Yan, L.; Chen, X.; He, Q.; Wang, Y.; Wang, X.; Guo, Q.; Bai, F.; Xia, A. Localized Emitting State and Energy Transfer Properties of Quadrupolar Chromophores and (Multi)Branched Derivatives. *J. Phys. Chem. A*, **2012**, *116*, 8693-8705.

7 Easwaramoorthi, S.; Thamaraiselvi, P; Duraimurugan, K.; Beneto, A.J.; Siva, A.; Nair, B.U. Charge Instability of Symmetry Broken Dipolar States in Quadrupolar and Octupolar Triphenylamine Derivatives *Chem. Commun.*, **2014**, *50*, 6902-6905.

8 Wan, Y.; Yan, L.; Zhao, Z.; Ma, X.; Guo, Q.; Jia, M.; Lu, P.; Ramos-Ortiz, G.; Maldonado, J.L.; Rodriguez, M.; Xia, A. Gigantic Two-Photon Absorption Cross Sections and Strong Two-Photon Excited Fluorescence in Pyrene Core Dendrimers with Fluorene/Carbazole as Dendrons and Acetylene as Linkages. *J. Phys. Chem. B*, **2010**, *114*, 11737-11745.

9 Wang, Y.; Yin, S.; Liu, J.; Yao, L.; Wang, G.; Liu, D.; Jing, B.; Cheng, L.; Zhong, H.; Shi, X. et al. Probing Ultrafast Excited State Dynamics and Nonlinear Absorption Properties of Three Star shaped Conjugated Oligomers with 1,3,5-Triazine Core. *RSC Adv.*, **2014**, *4*, 10960-10967.

10 Ramanan, C.; Kim, C.H.; Marks, T.J; Wasielewski, M.R. Excitation Energy Transfer within Covalent Tetrahedral Perylenediimide Tetramers and Their Intermolecular Aggregates. *J. Phys. Chem. C*, **2014**, *118*, 16941-16950.

11 Makarov, N.S.; Mukhopadhyay, S.; Yesudas, K.; Brédas, J.L.; Perry, J.W.; Pron, A.; Kivala, M.; Müllen, K.; Impact of Electronic Coupling, Symmetry, and Planarization on

Oneand Two-Photon Properties of Triarylamines with One, Two, or Three Diarylboryl Acceptors. *J. Phys. Chem. A*, **2012**, *116*, 3781-3793.

12 Montgomery, N.A.; Hedley, G.J.; Ruseckas, A.; Denis, J.C.; Schumacher, S.; Kanibolotsky, A.L; Skabara, P.J.; Galbraith, I.; Turnbull, G.A.; Samuel, I.D.W.; Dynamics of Fluorescence Depolarisation in Star-shaped Oligofluorene-Truxene Molecules. *Phys. Chem. Chem. Phys.*, **2012**, *14*, 9176-9184.

13 Zieschang, F.; Schmiedel, A.; Holzapfel, M.; Ansorg, K.; Engels, B.; Lambert, C.; Solvent Controlled Energy Transfer Processes in Triarylamine-Triazole Based Dendrimers. *J. Phys. Chem. C*, **2013**, *117*, 19816-19831.

14 Li, Y.; He, G.; Wang, X.; Guo, Q.; Niu, Y.; Xia, A. A Study of Excitation Delocalization/Localization in Multibranched Chromophores by Using Fluorescence Excitation Anisotropy Spectroscopy. *ChemPhysChem*, **2016**, *17*, 406 – 411.

15 Hu, J.; Li, Y.; Zhu, H.; Qiu, S.; He, G.; Zhu, X.; Xia, A.; Photophysical Properties of Intramolecular Charge Transfer in a Tribranched Donor–π–Acceptor Chromophore *ChemPhysChem*, **2015**, *16*, 2357-2365.

16 Li, Y.; Zhou, M.; Niu, Y.; Guo, Q.; Xia, A. Solvent-Dependent Intramolecular Charge Transfer Delocalization/Localization in Multibranched Push-Pull Chromophores. *J. Chem. Phys*., **2015**, *143*, 034309-1-034309-12.

17 Yang, W.; Li, C.; Zhang, M.; Zhou, W.; Xue, R.; Liu H.; Li, Y. Aggregation-induced emission and intermolecular charge transfer effect in triphenylamine fluorophores containing diphenylhydrazone structures. *Phys. Chem. Chem. Phys*. **2016**, *18*, 28052-28060.

18 Sissa, C.; Painelli, A.; Blanchard-Desce, M.; Terenziani, F; Fluorescence Anisotropy Spectra Disclose the Role of Disorder in Optical Spectra of Branched Intramolecular-Charge-Transfer Molecules. *J. Phys. Chem. B*, **2011**, *115*, 7009-7020.

19 Fonseca, R. D.; Vivas, M. G.; Luiz Silva, D.; Eucat, G.; Bretonnière, Y.; Andraud, C.; De Boni, L.; Mendonça, C. R. First-order Hyperpolarizability of Triphenylamine Derivatives Containing Cyanopyridine: Molecular Branching Effect. *J. Phys. Chem. C*, **2018**, *122*, 1770–1778.

20 Whitby, R.; Ben-Tal, Y.; MacMillan, R.; Janssens, S.; Raymond, S.; Clarke, D.; Jin, J.; Kay, A.; Simpson, M.C. Photoinitiators for Two-Photon Polymerisation: Effect of Branching and Viscosity on Polymerisation Thresholds. *RSC Adv*., **2017**, *7*, 13232–13239.

21 Parthasarathy, V.; Fery-Forgues, S.; Campioli, E.; Recher, G.; Terenziani, F.; Blanchard-Desce, M. Dipolar versus Octupolar Triphenylamine-Based Fluorescent Organic

Nanoparticles as Brilliant One- and Two-Photon Emitters for (Bio)imaging. *Small* **2011**, *7*, 3219–3229.

22 Li, B.; Tong, R.; Zhu, R.; Meng, F.; Tian, H.; Qian, S. The Ultrafast Dynamics and Nonlinear Optical Properties of Tribranched Styryl Derivatives Based on 1,3,5-Triazine. *J. Phys. Chem. B*, **2005**, *109*, 10705-10710.

23 Gao, Y.; Qu, Y.; Jiang, T.; Zhang, H.; He, N.; Li, B.; Wu, J.; Hua, J. Alkyl-triphenylamine End-Capped Triazines with AIE and Large Two-Photon Absorption Cross-Sections for Bioimaging. *J. Mater. Chem. C*, **2014**, *2*, 6353-6361.

24 Montgomery, N.A.; Denis, J.C.; Schumacher, S.; Ruseckas, A.; Skabara, P.J.; Kanibolotsky, A.; Paterson, M.J.; Galbraith, I.; Turnbull, G.A.; Samuel, I.D.W. Optical Excitations in Star-Shaped Fluorene Molecules. *J. Phys. Chem. A*, **2011**, *115*, 2913-2919.

25 Yuan, M.S.; Wang, Q.; Wang, W.J.; Li, T.B.; Wang, L.; Deng, W.; Du, Z.T.; Wang, J.R. Symmetrical and Asymmetrical (Multi)Branched Truxene Compounds: Structure and Photophysical Properties. *Dyes Pigm.*, **2012**, *95*, 236-243.

26 Du, X.; Yuan, M.S.; Xu, F.; Wang, H.; Wang, Q.; Wang, W.; Wang, D.E.; Wang, J. Branched Truxene and Triindole Compounds and Their Solid-State Luminescent Enhancement. *Spectrochimica Acta Part A: Molecular and Biomolecular Spectroscopy* **2016**, *164*, 33–39.

27 He, G.; Shao, J.; Li, Y.; Hu, J.; Zhu, H.; Wang, X.; Guo, Q.; Chi, C.; Xia, A. Photophysical Properties of Octupolar TriazatruxeneBased Chromophores. *Phys. Chem. Chem. Phys.*, **2016**, *18*, 6789-6798.

28 Bordeau, G.; Lartia, R.; Metge, G.; Fiorini-Debuisschert, C.; Charra, F.; Teulade-Fichou, M.P. Trinaphthylamines as Robust Organic Materials for Two-Photon-Induced Fluorescence *J. Am. Chem. Soc.* **2008**, *130*, 16836–16837.

29 Bhaskar, A.; Ramakrishna, G.; Lu, Z.; Twieg, R.; Hales, J. M.; Hagan, D. J.; Van Stryland, E.; Goodson, T. Investigation of Two-Photon Absorption Properties in Branched Alkene and Alkyne Chromophores. *J. Am. Chem. Soc.* **2006**, *128*, 11840-11849.

30 Schmitt, V.; Moschel, S.; Detert, H. Diaryldistyrylpyrazines: Solvatochromic and Acidochromic Fluorophores *Eur. J. Org. Chem.* **2013**, 5655–5669.

31 Zhang, Q.; Luo, L.; Xu, H.; Hu, Z.; Brommesson, C.; Wu, J.; Sun, Z.; Tian, Y.; Uvdald, K. Design, Synthesis, Linear and Nonlinear Photophysical Properties of Novel Pyrimidine-Based Imidazole Derivatives. *New J. Chem.*, **2016**, *40*, 3456-3463.

32 Chen, D.; Zhong, C.; Zhao, Y.; Nan, L.; Liuc, Y.; Qin J. A Two-Dimensional Molecule with Large Conjugation Degree: Synthesis, Two-Photon Absorption and Charge Transport Ability. *J. Mater. Chem. C*, **2017**, *5*, 5199-5206.

33 Achelle, S.; Nouira, I.; Pfaffinger, B.; Ramondenc, Y.; Plé, N.; Rodríguez-López, J. V-Shaped 4,6-Bis(arylvinyl)pyrimidine Oligomers: Synthesis and Optical Properties. *J. Org. Chem.*, **2009**, *74*, 3711–3717.

34 Tydlitát, J.; Achelle, S.; Rodríguez-López, J.; Pytela, O.; Mikysek, T.; Cabon, N.; Robin-le Guen, F.; Miklík, D.; Růžičková, Z.; Bureš, F. Photophysical Properties of Acid-Responsive Triphenylamine Derivatives Bearing Pyridine Fragments: Towards White Light Emission. *Dyes Pigm.*, **2017**, *146*, 467-478.

35 Achelle, S.; Rodríguez-López, J.; Katan, C.; Robin-le Guen, F. Luminescence Behavior of Protonated Methoxy-Substituted Diazine Derivatives: Towards White Light Emission. *J. Phys. Chem. C*, **2016**, *120*, 26986−26995.

36 Achelle, S.; Rodríguez-López, J.; Cabon, N.; Robin-le Guen, F. Protonable Pyrimidine Derivative for White Light Emission. *RSC Adv.*, **2015**, *5*, 107396-107399.

37 Liu, D.; Zhang, Z.; Zhang. H.; Wang, Y. A Novel Approach Towards White Photoluminescence and Electroluminescence by Controlled Protonation of a Blue Fluorophore. *Chem. Commun.*, **2013**, *49*, 10001-10003.

38 Li, M.; Yuan, Y.; Chen. Y. Acid-induced Multicolor Fluorescence of Pyridazine Derivative. *ACS Appl. Mater. Interfaces*, **2018**, *10*, 1237–1243.

39 Giovanella, U.; Cariati, E.; Lucenti, E.; Pasini, M.; Galeotti, F.; Botta, C. In Situ Electroluminescence Color Tuning by Thermal Deprotonation Suitable for Thermal Sensors and Anti-Fraud Labels. *ChemPhysChem* **2017**, *18*, 2157-2161.

40 Hancock, J. M.; Jenekhe, S. A. Unusual Protonation-Induced Continuous Tunability of Optical Properties and Electroluminescence of a π-Conjugated Heterocyclic Oligomer. *Macromolecules*, **2008**, *41*, 6864-6867.

41 Huynh, H. V; He, X.; Baumgartner, T. Halochromic Generation of White Light Emission Using a Single Dithienophosphole Luminophore. *Chem. Commun.*, **2013**, *49*, 4899-4901.

42 Romero-Nieto, C.; Durben, S.; Kormos, I. M.; Baumgartner, T. Simple and Efficient Generation of White Light Emission From Organophosphorus Building Blocks. *Adv. Funct. Mater.*, **2009**, *19*, 3625–3631.

43 Seintis, K.; Agathangelou, D.; Cvejn, D.; Almonasy, N.; Bureš, F.; Giannetas, V.; Fakis, M. Femtosecond to Nanosecond Studies of Octupolar Molecules and Their Quadrupolar and Dipolar Analogues. *Phys. Chem. Chem. Phys.*, **2017**, *19*, 16485-16497.

44 Karakostas, N.; Martinou, E.; Kaloudi-Chantzea, A.; Seintis, K.; Oberacher, H.; Pitterl Florian, F.; Fakis, M.; Kallitsis, J. K.; Pistolis, G. Energy Transfer within Self-Assembled Cyclic Multichromophoric Arrays Based on Orthogonally Arranged Donor - Acceptor Building Blocks. *Faraday Disc.*, **2015**, *185*, 433-454.

45 Fakis, M.; Stathatos, E.; Tsigaridas, G.; Giannetas, V.; Persephonis, P. Femtosecond Decay and Electron Transfer Dynamics of the Organic Sensitizer D149 and Photovoltaic Performance in Quasi-Solid-State Dye-Sensitized Solar Cells. *J. Phys. Chem. C*, **2011**, *115*, 13429-13437.

46 Kaloudi-Chantzea, A.; Martinou, E.; Seintis, K.; Karakostas, N.; Giastas, P.; Pitterl, F.; Oberacher, H.; Fakis, M.; Pistolis, G. A Highly – Ordered Rigid Multichromophoric 3D Supramolecular Network by Combining Ionic and Coordination – Driven Self – Assembly. *Chem. Commun.*, **2016**, *52*, 3388-3391.

47 Droseros, N.; Seintis, K.; Fakis, M.; Gardelis, S.; Nassiopoulou, A. Steady State and Time Resolved Photoluminescence Properties of CuInS2/ZnS Quantum Dots in Solutions and in Solid Films *J. Lumin.*, **2015**, *167*, 333-338.

48 Terenziani, F.; Le Droumaguet, C.; Katan, C.; Mongin, O.; Blanchard-Desce, M. Effect of Branching on Two-Photon Absorption in Triphenylbenzene Derivatives. *ChemPhysChem*, **2007**, *8*, 723-734.

49 Dereka, B.; Vauthey, E. Solute-Solvent Interactions and Excited-State Symmetry Breaking: Beyond the Dipole-Dipole and the Hydrogen-Bond Interactions. *J. Phys. Chem. Lett*. **2017**, *8*, 3927–3932.

50 Dereka, B.; Rosspeintner, A.; Stężycki, R.; Ruckebusch, C.; Gryko, D. T.; Vauthey, E. Excited-State Symmetry Breaking in a Quadrupolar Molecule Visualized in Time and Space. *J. Phys. Chem. Lett.* **2017**, *8*, 6029–6034.

51 Taft, R. W.; Kamlet, M. J. The Solvatochromic Comparison Method. 2. The Alpha.-Scale of Solvent Hydrogen-Bond Donor (HBD) Acidities. *J. Am. Chem. Soc*. **1976**, *98*, 2886-2894.

52 Davydov, A.S. Theory of Molecular Excitons, Plenum Press, New York, 1971.

53 Beljonne, D.; Wenseleers, W.; Zojer, E.; Shuai, Z.; Vogel, H.; Pond, S.J.K.; Perry, J.W.; Marder, S.R.; Brédas, J.L. Role of Dimensionality on the Two-Photon Absorption Response of Conjugated Molecules: The Case of Octupolar Compounds. *Adv. Funct. Mater*., **2002**, *12*, 631-641.

54 Lewis, J.E.; Maroncelli, M. On the (Uninteresting) Dependence of the Absorption and Emission Transition Moments of Coumarin 153 on Solvent. *Chem. Phys. Lett.*, **1998**, *282*, 197-203.

55 He, G.; Yu, C.; Li, Y.; Hu, J.; Liu, Z.; Zhang, D.; Guo, Q.; Xia, A. Excitation Energy Transfer in meta-Substituted Phenylacetylene Multibranched Chromophores. *Chem. Asian J.*, **2016**, *11*, 2741–2748.

56 Sluch, M. I.; Godt, A.; Bunz, U. H. F.; Berg, M. A. Excited-State Dynamics of Oligo(p-phenyleneethynylene): Quadratic Coupling and Torsional Motions. *J. Am. Chem. Soc.*, **2001**, *123*, 6447-6448.

57 Jiang, J.; Alsam, A.; Wang, S.; Aly, S.M.; Pan, Z.; Mohammed, O. F.; Schanze, K. S. Effect of Conjugation Length on Photoinduced Charge-Transfer in π-Conjugated Oligomer-Acceptor Dyads. *J. Phys. Chem. A*, **2017**, *121*, 4891–4901.

58 Sissa, C.; Parthasarathy, V.; Drouin-Kucma, D.; Werts, M. H. V.; Blanchard-Desce, M.; Terenziani, F. The Effectiveness of Essential-State Models in the Description of Optical Properties of Branched Push–Pull Chromophores. *Phys. Chem. Chem. Phys.*, **2010**, *12*, 11715-11727.

59 Teranziani, F.; Sissa, C.; Painelli, A. Symmetry Breaking in Octupolar Chromophores: Solvatochromism and Electroabsorption. *J. Phys. Chem. B*, **2008**, *112*, 5079-5087.

60 Lippert, E. *Z. Naturforsch. A*, **1955**, *10*, 541-545.

61 Mataga, N.; Kaifu, Y.; Koizumi, M. The Solvent Effect on Fluorescence Spectrum. Change of Solute-Solvent during the Lifetime of Excited Solute Molecule. *Bull. Chem. Soc. Jpn.*, **1955**, *28*, 690-691.

62 Hall, R. D.; Valeur, B.; Weber, W. Polarization of the Fluorescence of Triphenylene. A Planar Molecule With Three-Fold Symmetry. *Chem. Phys. Lett.*, **1985**, *116*, 202-205.

63 Campo, J.; Painelli, A.; Terenziani, F.; Regemorter, T. V.; Beljonne, D.; Goovaerts, E.; Wenseleers, W. First Hyperpolarizability Dispersion of the Octupolar Molecule Crystal Violet: Multiple Resonances and Vibrational and Solvation Effects. *J. Am. Chem. Soc.*, **2010**, *132*, 16467-16478.

64 Ishow, E.; Clavier, G.; Miomandre, F.; Rebarz, M.; Buntinx, G.; Poizat, O. Comprehensive Investigation of the Excited State Dynamics of Push-Pull Triphenylamine Dyes as Models for Photonic Applications. *Phys. Chem. Chem. Phys.*, **2013**, 15, 13922-13939.

65 Horng, M.L.; Gardecki, J.A.; Papazyan, A.; Maroncelli, M. Subpicosecond Measurements of Polar Solvation Dynamics: Coumarin 153 Revisited. *J. Phys. Chem.*, **1995**, *99*, 17311–17337.

66 Varnavski, O.; Goodson III, T; Sukhomlinova, L.; Twieg, R. Ultrafast Exciton Dynamics in a Branched Molecule Investigated by Time-Resolved Fluorescence, Transient Absorption, and Three-Pulse Photon Echo Peak Shift Measurements. *J. Phys. Chem. B*, **2004**, *108*, 10484-10492.

67 Wang, Y.; Ranasinghe, M. I.; Goodson III, T. Ultrafast Fluorescence Investigation of Excitation Energy Transfer in Different Dendritic Core Branched Structures. *J. Am. Chem. Soc*., **2003**, *125*, 9562-9563.

68 Varnavski, O.P.; Ostrowski, J.C.; Sukhomlinova, L.; Twieg, R.J.; Bazan, G.C.; Goodson III, T. Coherent Effects in Energy Transport in Model Dendritic Structures Investigated by Ultrafast Fluorescence Anisotropy Spectroscopy. *J. Am. Chem. Soc*., **2002**, *124*, 1736-1743.

69 Gudeika, D.; Grazulevicius, J.V.; Volyniuk, D.; Juska, G.; Jankauskas, V.; Sini, G. Effect of Ethynyl Linkages on the Properties of the Derivatives of Triphenylamine and 1,8-Naphthalimide. *J. Phys. Chem. C*, **2015**, *119*, 28335-28346.

70 Lacowicz, J.R. Principles of Fluorescence Spectroscopy, Springer, 2006.

71 Pullerits, T.; Hess, S.; Herek, J. L.; Sundström, V. Temperature Dependence of Excitation Transfer in LH2 of Rhodobacter sphaeroides. *J. Phys. Chem. B*, **1997**, *101*, 10560-10567.

72 Valeur, B. Molecular Fluorescence: Principles and Applications. 2001 Wiley-VCH Verlag GmbH.

73 Bures, F.; Cvejn, D.; Melánová, K.; Beneš, L.; Svoboda, J.; Zima, V.; Pytela, O.; Mikysek, T.; Růžičková, Z.; Kityk, I. V. et al. Effect of Intercalation and Chromophore Arrangement on the Linear and Nonlinear Optical Properties of Model Aminopyridine Push–Pull Molecules. *J. Mater. Chem. C*, **2016**, *4*, 468-478.

TOC Graphic

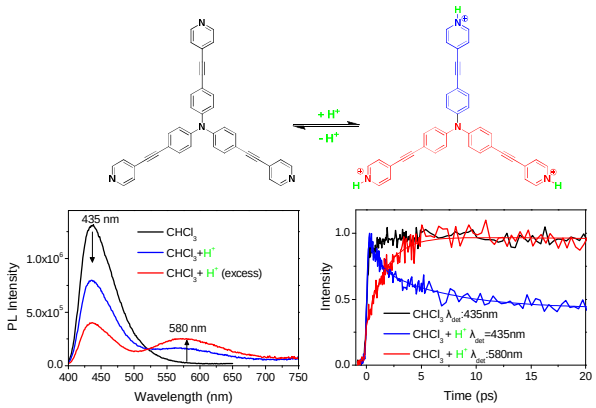
+ H+
- H+
435 nm
580 nm
CHCl3
CHCl3+H+
CHCl3+ H+ (excess)
PL Intensity
Wavelength (nm)
CHCl3 λdet:435nm
CHCl3 + H+ λdet=435nm
CHCl3 + H+ λdet:580nm
Intensity
Time (ps)